Metrologia
Fortaleza - CE 2017

Image Preprocessing Techniques and Finite Element Methods Applied to Flatness Measurement Automation

Ricardo dos Santos França [1], Ayrton Maia Rocha da Cunha [2]

[1] Laint/Diopt/Dimci/Inmetro; [2] DEL/UFRJ

E-mail: rsfranca@inmetro.gov.br

Abstract: A new approach to automate 2D interferometric flatness deviation (FD) measurements is developed. A Finite Element Method (FEM) technique allows height map estimations from phase reconstruction of digitized Fizeau type interferograms. An algorithm computes local phase values by a least-squares fit from preprocessed interferograms, partitioned by FEM into a small triangle elements pattern inside a circular mask. Those local linear phase variations are combined into a global map by phase unwrapping and tilt plane removal steps. Flatness deviation of optical surfaces is evaluated from height variations obtained by this final map, with reduced uncertainties in comparison with previous measurement methods.

Keywords: Flatness deviation, Interferometry, Length metrology, Finite-element methods, Phase estimation.

1. INTRODUCTION

Well-established visual estimation techniques used in old and reliable measurement systems are been replaced by automated systems used in length interferometry metrology labs [1]. Typical approaches include phase shift interferometry, model profile direct fit with Zernike coefficients, Fourier phase extraction, etc. [2]. However, those methods either require additional hardware or are computationally intensive for real lab application.

Surface flatness values are evaluated from global height variations, deduced from 2D phase displacement info embedded in interferometric images. The best metrological algorithms used for those measurements are based on a good balance between idealized models and the actual measured profiles, as feasible and accurate approximations of interferometric parameters from arbitrary surfaces are usually associated to large execution times.

Moreover, several of foremost estimation algorithms perform poorly with ill-conditioned input data or when it is almost undistinguished from random and systematic noise. Therefore, it is of paramount importance to apply suitable data pre-processing steps before operation of such noise sensitive algorithms.

Finite Element Methods (FEM) are well-known as fast computation and general purpose techniques to model various physical property maps. However, their noise sensitivity and the complexity of several actual interferometric patterns presented us the challenge to use them at practical flatness interferometry measurements.

Since FEM are highly noise-sensitive methods, intelligent pre-filtering and pre-processing techniques are required to de-noise actually captured images. Otherwise, a preprocessing-free set of simulation-generated interferograms should be tested before any further algorithm validation.

2. FLATNESS INTERFEROMETRY TECHNIQUES AND SYSTEMS UPGRADE

2.1. Fizeau interferometer

The interferometer still used to perform all regular flatness deviation calibrations in Inmetro (Brazilian National Metrology Institute) is an old Fizeau-type interferometer, fitted with a Thallium spectral lamp as its length unit reference, due to its ongoing reliability and easy operation. As first upgrade to develop automated measurement algorithms, a high-resolution and time-exposition-controlled digital-interfaced CCD camera was attached at interferometer rear port to expand overall resolution and reduce measurement uncertainties.

2.2. Phase-shifter interferometers

Modern commercial interferometers are designed to include phase-shift subsystems. Those produce optical path controlled variations, and whole sequential 2D interferogram snapshots, that produce local sinusoidal intensity patterns in each individual pixel and its phase information [1]. Height maps are reconstructed from individual pixel values at several phase steps [2,3,4]. While a phase-shifting method has its advantages, as immunity to optical noises and good reproduction of actual height variations, it needs extensive hardware and is not always possible to implement it with all-optical old interferometers.

2.3. Phase estimation automation strategies

The first automation strategy was to use a skeletonizing method, using a geometric estimation of fringe image maxima intensity points and following a similar procedure as used by traditional visual fringe curvature estimation. Unfortunately, this method needs surface height variations with almost perfect spherical symmetry. The next approach was based in assuming height variation modeling through polynomial-defined curvature ideal surfaces. Parameter search techniques were executed to find minimum-error surface maps, by stochastic-plus-deterministic methods. Similar approaches were tried with good reliability at closely related metrological applications, but because some global relief maps cannot be approximated by abstract mathematic surfaces, a more accurate local/global method was needed.

For that goal a hybrid Finite-Element-Method approach was originally developed to test known height variations templates as defined by simulated interferograms, and afterwards applied to images obtained from actual optical surfaces.

3. NEW ALGORITHM STEPS

3.1. Image preprocessing

Local image outliers coming from surface roughness or abrupt intensity variations due to small scratches, optical spots or camera artifacts must be pre-filtered before applying the designed noise-sensitive FEM estimation algorithms.

A suitable preprocessing technique was to apply Fourier transform on 2D image and pass it by a high-order low-pass Butterworth 2D filter, to remove the roughness and rich-noise higher frequency components. These kind of maximum homogeneity filters don't add significant flatness-information distortion on lower frequency components. After an inverse-transformed FFT, a predefined number of horizontal, vertical and circular lines are fixed, and local maximal points in the smoothed interferogram have their coordinates and intensities searched and marked. A 2D cubic spline interpolation then equalizes remaining intensity fluctuations due to finite area sampling and numerical artifacts near border regions. A final zeroing mask cut out remaining artifacts in regions beyond its border, delimiting a feasible circular measurement area.

However, we can skip those steps by using in next phases noise-free simulated interferograms.

3.2. Finite-Element Method

After preprocessing the interferogram, we can obtain its local phase variation map through a FEM scan strategy.

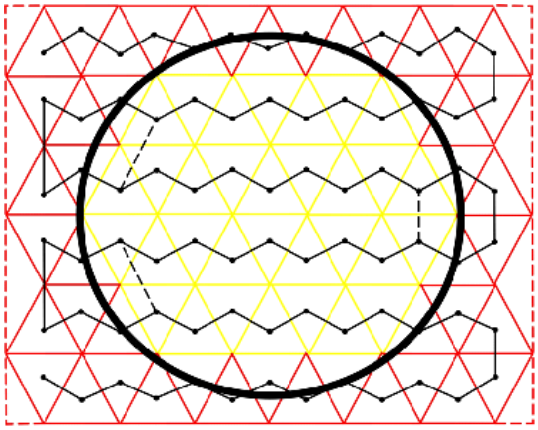

Figure 1. Triangle masked partition and scan pattern used in finite-element local phase parameter estimation.

Figure 1 shows a masked partition modeling for the whole image, built upon an almost regular triangle predefined mesh. Local linear phase and spatial frequency parameters are estimated by fast least squares parameter search techniques, executed independently for each small triangle at linear scanned patterns. The automated partition identifies feasible (yellow) from unfeasible triangles (red), whereas all feasible vertices are positioned inside the circular boundary.

3.3. Phase unwrapping and overall linear phase plane compensation

Local phase contributions computed from each feasible triangle must be composed and fed on the next fast scanned phase-unwrapping and accurate linear phase plane compensation steps.

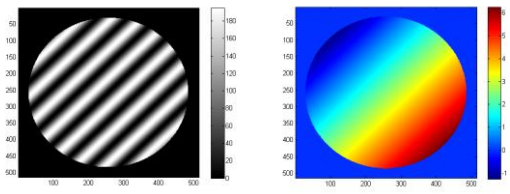

Figure 2. Interferogram and its linear phase plane

The phase jump rectification and unwrapping steps are made by successive neighborhood comparisons of the scanned triangle centers, resulting in a smooth phase variation map. A least squares fit gives the parameters of a global linear phase plan to be subtracted from all local linear phase variations, as in figure 2, to produce the global phase deviation map. Such phase plane is due to the physical parallelism deviation between measurement and reference surfaces, whose tilting is needed to produce a suitable fringe amount for a reliable algorithm operation.

4. TESTS AND RESULTS

To evaluate the algorithm performance a homogeneous circular-cut zero-FD simulated interferogram, used as a no-preprocessed image having $f_x = 5$ and $f_y = 6$ as spatial frequencies, was partitioned by our FEM algorithm. Its global flatness deviation estimated value of 6.4 nm, as also values from other designed lorentzian profile hills, their predefined height reference values (RV) positioned within a hypothetical 40 mm diameter of circular mask, their approximated values (AV) and their differences (DV) in nanometers can be seen in table 1.

Table 1. Designed (RV) and approximated (AV) FD values, with their differences (DV).

RV (nm)	AV (nm)	DV (nm)
0	6.4	6.4
50	48.2	1.8
116	129.0	13.0
252	248.7	3.3
387 (I)	273.5	113.5
395 (II)	346.6	48.4

Those DV differences were strongly height-independent, and their variation was mainly caused by distinct profile form and peak positioning of simulated hills. The last two rows of table 1 are related to hills with maxima heights positioned on mask borders. The last DV (II) showed a remarkable improvement compared

with its predecessor (I) due to a late upgrade in first algorithm version, as the older version was too sensitive to large phase variations near the circular border. This last value is still greater than Inmetro's best old expanded uncertainty value of ± 30 nm, our current acceptance goal upper bound for this FEM method.

Figure 3a depicts the last simulated fringe interferogram. The lower–right local distortion on dark-bright spacing is related to the previously designed height variation. Figure 3b shows a false color height map profile obtained after FEM, phase unwrap and tilt compensation operations.

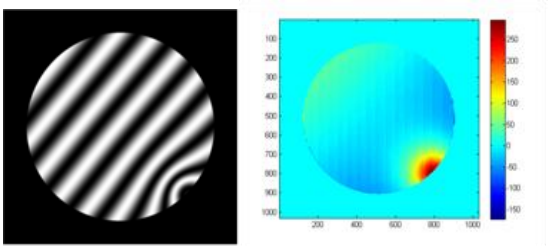

(a) (b)

Figure 3. Images of a simulated interferogram (a), and its approximated 347 nm height variation (b)

Strong sensitivity effects due to slightly incomplete carrier frequency / linear phase plane least-square compensation, are caused by no-centered and/or no-symmetrical hills, and they contributed to the larger differences shown above. A technique to reduce those effects can be seen in [5] and it can be embedded in a future upgraded version of current FEM algorithm.

If nominal flatness deviation values of optical flats are less than 300 nm, we can adopt a first combined uncertainty lower value of circa ± 15 nm. That value may comprise all FEM algorithm uncertainty contributions due to partitioning, compensation and pre-processing denoising steps. Inaccuracies due to minimum triangle sizes and partial covering of feasible area within circular mask are still smaller than those due to inaccurate linear phase plane compensation.

5. CONCLUSIONS AND FUTURE DEVELOPMENTS

Several artificial interferograms with known flatness deviations were generated to compare results obtained by a designed FEM strategy. The 6.4 nm value for a zero-FD could be considered as the first experimental uncertainty lower boundary for this method. Higher FDs and height profile asymmetries resulted in differences between designed and obtained FDs. The algorithm accuracy should be tested over real-life surface standards with previously measured FD values. A comparative discussion must still follow about further results from automated phase estimations by stochastic methods, based on images digitized from Fizeau interferometer, or by measurements by a half-automated phase-shifter interferometer, on same optical flats.

As the current best measurement capability declared for Inmetro's flatness measurement uncertainties is ± 30 nm (k = 2), we assume that further developments on this new FEM algorithm would show remarkable improvements over its current flatness measurement uncertainty values.

6. REFERENCES

[1] Narumi T *et al* 1998 Development of New Automatic Gauge Block Interferometer up to 250 mm *Proc. SPIE Repr.* San Diego California July/1998

[2] Malacara D 2007 *Optical Shop Testing* 3rd edition John Wiley & Sons

[3] Hack E and Burke J 2011 Measurement uncertainty of linear phase-stepping algorithms *Rev. Sci. Instr.* **82** 061101

[4] Malinovski I *et al* 2016 *Surf. Topogr.: Metrol. Prop.* **4** 024006

[5] Quan C *et al* 2007 *Opt. Laser Technol.* **39** 1155–1161